Applied Physics A (2022) 128:56
https://doi.org/10.1007/s00339-021-05196-z

Applied Physics A
Materials Science & Processing

Utilizing dip-coated graphene/nanogold to enhance SPR-based fiber optic sensor

Mahmoud Gomaa[1] · **Abeer Salah**[1] · **Gamal Abdel Fattah**[1]

Received: 8 September 2021 / Accepted: 7 December 2021

Abstract
Optical fiber sensing is an important sensing technique where combining the advantage of using new materials such as graphene and the features of the optical fibers. Previously, the sensing probes were prepared by different methods such as sputtering; we are seeking for a new, easy, low-cost and not complicated method with superior advantages over other methods. In this paper, dip-coated sensing probes of gold film (Au), graphene/gold film/core (Gn/Au/core), gold nanoparticles/core (AuNPs/core) and graphene/gold nanoparticles/core (Gn/AuNPs/core) are prepared. The structures of probes were examined via scanning electron microscope and Raman spectroscopy. In the Gn/AuNPs/core structure, the Gn surface and AuNP surface are rough enough to increase the surface area of the sensor. Lead ions in water with different concentrations were detected via optical fiber surface plasmon resonance with the prepared probes. Sensor performance parameters for the fabricated probes were calculated. The Gn/AuNPs/core probe shows a superior sensitivity (Sn), figure of merit, signal-to-noise ratio and limit of detection among other sensors, which make it available for chemical and biological applications. In this work, the dip-coated graphene is a promising method for enhancing performance parameters of optical fiber sensors, not complicated, low cost and easy in comparison with commonly used sputtering method.

Keywords Fiber optic sensor · Surface plasmon resonance · Graphene · Dip coating method

1 Introduction

Surface plasmon resonance (SPR) is a highly sensitive optical sensing technique used to detect small changes in the effective metal–dielectric interface refractive index in real time [1]. SPR usually refers to the coupling of the electromagnetic wave with the surface plasmon wave (SPW) on the interface between the metal and the dielectric medium, and this coupling causes a decrease in the reflected intensity [2]. There are a number of techniques for SPR sensor excitation monitoring, such as intensity [3], angle [4], phase [5] and wavelength interrogation [6]. Angle-based interrogation sensors suffer from operating at a single wavelength and mechanical movement, and cannot be used for remote control applications [7–9]. Due to these disadvantages, many researchers have used the core of an optical fiber instead of prism to address these limitations [10]. Recently, optical fiber sensors have been gaining interest due to their unique advantages such as low attenuation, extremely fast response, small size, low cost, label-free samples, real-time analysis, remote sensing and high-performance parameters [11–14]. Optical fiber surface plasmon resonance (SPR) sensor uses the surface plasmon waves (SPW) at the interface between a metal and dielectric to sense the interactions between sensing medium and the metal surface [15–17]. A change in the concentration of the sensing medium will produce a change in refractive index, which result in a redshift in the resonance wavelength [18]. Optic fiber SPR sensors are fabricated by uncladded core of a small portion of optical fiber; then, metals (usually gold or silver) are coated on the unclad core [19–22]. But, the poor adsorption of biomolecules on gold and the easy oxidation of silver are limiting the sensitivity of fiber optic sensors (FOS) [23, 24]. In order to improve the sensitivity of fiber optic SPR sensors, there were various attempts have been proposed [25].

Graphene recently emerged as another alternative for enhancing the sensitivity of different types of biosensors [26]. Owing to excellent features of graphene, it can be a very

✉ Mahmoud Gomaa
mdgomaa@niles.edu.eg

[1] Department of Laser Sciences and Interactions, National Institute of Laser Enhanced Sciences, Cairo University, Giza 12613, Egypt

Published online: 21 December 2021

promising candidate as a sensing layer for fiber optic sensors [27]. The addition of graphene layer over metals improves the sensitivity of the biosensor and prevents oxidation in the other layers [28, 29]. Graphene has very fascinating properties such as zero band gap, two-dimensional structure, high electron mobility, lowest resistivity and the mobility for charge carriers [30, 31]. Also owing to its large surface-to-volume ratio and π-stacking interactions between graphene and biomolecules, it can effectively absorb a variety of polar molecules and biomolecules [32, 33]. However, transferring single layer via chemical vapor deposition of graphene onto metal surface-coated core of optical fiber is still a big challenge. In addition, metal coating via sputtering has numerous shortcomings such as a complex and an expensive equipment to ensure that the metal film uniformity and the biomolecules adsorb poorly on these metals. To solve this problem effectively, we proposed the dip coating method for coating graphene onto metals surfaces on the optical fiber core. Graphene suspension has been prepared by microwave plasma chemical vapor deposition (MWPCVD) as in our previous work [34]. In dip coating method, the probe was then immersed in graphene suspension for the formation of graphene layer on the surface of the metals.

As far as we know, there are no experimental studies on graphene coating as a sensing layer over metals by the dip coating method. In this paper, fabricated sensor probes of dip-coated graphene are compared to Au/core and AuNPs/core probes. The graphene/Au/core and graphene/AuNPs/core fiber optic SPR sensors show higher sensitivity in comparison with Au/core and AuNPs/core fiber optic SPR sensors. The sensor performance is analyzed in terms of parameters: sensitivity, signal-to-noise ratio (SNR), figure of merit (FOM) and limit of detection (LOD) for different concentrations of lead ions in water. It is the first time to verify that the dip-coated graphene enhances the performance of sensor experimentally. SPR fiber optic with dip-coated graphene increases sensitivity and figure of merit (FOM) of fiber optic sensors (FOS).

2 Experimental details

2.1 Probe preparations

For the fabrication, 25 cm of optical fiber was used; the fiber optic SPR probe was manufactured with a 200 µm silica core diameter and a 250 µm polymer cladding diameter of a multimode optical fiber (Newport FC-2UVC-100). Fiber probe ends were sufficiently polished to improve the light coupling by abrasive paper with a roughness of 4°.

At the center of 25 cm of optical fiber, 1 cm of the outer jacket and the polymer cladding of the optical fiber were removed by flame heating. The unclad region was cleaned by hydrofluoric (HF) acid to remove the residual plastic, was easily rinsed with acetone and then deionized water to remove any residues without any treatment as shown in Fig. 1a, b.

2.1.1 Sputtered gold thin film–fiber probe (Au/core)

We used the bare core prepared in Sect. 2.1 for depositing gold layer by sputtering, and DC magnetron was used for sputtering gold (gold target: 99.9% pure). The fiber probes were placed on a glass slide at a distance of 8 cm from the gold target, allowing sputter deposition only on the unclad region as shown in Fig. 1c. The fiber rotated by angle 180° and deposition of gold repeated with the same conditions. Gold deposition was done at current 25 mA and time 210 s. According the calibration of (S150A SPUTTER COATER) at this current and time, the deposited thickness on surface of the bare core of optical fiber is about 40–50 nm. The deposition and uniformity of sputtered gold on the bare core of optical fiber are examined by optical microscope, Raman spectroscopy and scanning electron microscope (SEM).

2.1.2 Gold nanoparticles–fiber probe (AuNPs/core)

In this case, the gold nanoparticles were prepared by the citrate reduction method as mentioned in [35]; trisodium citrate as capping and reducing agent was added to the boiling gold precursor ($HAuCl_4$) solution under stirring until it turns red. After the gold colloids turned red, the temperature was switched off and the solution was stirred for 10 min, resulting in gold nanoparticles solution. Gold nanoparticle solution was characterized by UV–Vis absorption spectroscopy. The Au nanoparticles probe is prepared by dip coating method via the deposition of gold nanoparticles on the optical fiber core. At room temperature, the fiber was dipped in the gold nanoparticle solution for 48 h. The AuNP coating on the optical fiber core is examined by Raman spectroscopy and scanning electron microscope (SEM).

2.1.3 Graphene–fiber probes (Gn/Au/core) and (Gn/AuNPs/core)

In our previous research, graphene suspension is synthesized using microwave plasma chemical vapor deposition technique and characterized by different techniques [34, 36]. The deposition of the nanostructured graphene (Gn) by dip coating

Fig. 1 Schematic for (**a**) optical fiber, (**b**) unclad region before deposition, (**c**) unclad region after gold deposition

method onto the optical fiber core pre-sputtered with gold film or pre-dip-coated gold nanoparticles is achieved. Probes coated with Au film and dip coating Au nanoparticles were prepared in Sects. 2.1.1 and 2.1.2, respectively. These probes were immersed in the graphene suspension. The fiber and formed graphene layer on the surface were placed in a 50 °C oven for 1 h. The coated probes with Gn was left overnight to further enhance the formation of thin film on the surface prior to use. The prepared probes are studied using Raman spectroscopy and scanning electron microscope (SEM) to examine the morphology of graphene deposition on Au/core and AuNPs/core probes.

2.2 Preparation of lead stock solution

Lead (II) nitrate ($Pb(NO_3)_2$) is used as the source of lead stock solution. 1.615 g of 99% $Pb(NO_3)_2$ is dissolved in distilled water in a 1-L volumetric flask up to the mark to obtain 1000 ppm (mg/L) of lead stock solution. Different concentrations of lead ions (0, 5,10,30,50,100 and 200 ppm) are prepared from this stock solution by appropriate dilutions according to equation dilution [37].

$$C_1V_1 = C_2V_2 \quad (1)$$

where C_1 and C_2 are initial and desired concentrations, respectively, and V_1 and V_2 are the initial and desired volumes, respectively.

The fiber optic probe structures were used to detect different concentrations of lead ion solutions.

2.3 Experimental setup

The experimental setup using the optical fiber SPR sensor for sensing different concentrations of lead ions in water is shown in Fig. 2, where sensing lead ions in water were measured in a sensing cell (chamber) with the fiber probe mounted along its center axis. Electrical pump was used to circulate the solution in the cell, and the solution flowed through the cell with flow rate (5.5 mL/sec). A tungsten–halogen lamp was used as a light source (spectrum range of 400–1000 nm). Light passes through a monochromator and polarizer and was focused onto the input face of the optical fiber probe to couple light into the fiber with the help of a microscope objective and fiber coupler. The other end of the optical fiber probe was connected to the photomultiplier tube detector. The transmission spectra were measured in 400–800 nm wavelength range. The SPR spectra were recorded for different concentrations of lead ions in water at room temperature. The resonance wavelengths and performance parameters corresponding to different concentrations of lead ions were determined from the SPR spectra. After each measurement, the fiber optic probe was washed with distilled water and dried to remove any residual from the last measurement.

3 Results and discussions

3.1 Sensor fabrication results

The UV–Vis absorption spectrum of AuNPs as prepared is shown in Fig. 3. A broad absorption peak at 525 nm is due to the characteristic surface plasmon resonance absorption of gold nanoparticles. Dip coating method was used to deposit AuNPs on a bare core of optical fiber. Au film was deposited on the bare core of other sample by sputtering method. Then the Gn was deposited on both Au and AuNP surfaces of the two samples by dip coating method and then dried in 50 °C for 1 h in oven.

Scanning electron microscope images are shown in Fig. 4a–e. Figure 4a shows the surface of fiber optic bare core before any deposition, it seems as smooth as it is appeared. After Au deposited by sputtering, the smooth surface is again obtained as shown in Fig. 4b. Figure 4c shows the deposited Gn faint layer by dip coating on the

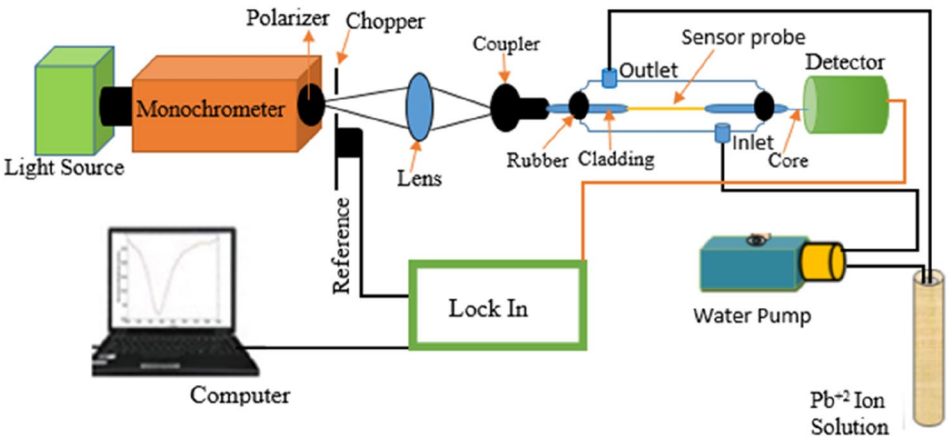

Fig. 2 Schematic diagram of the experimental setup

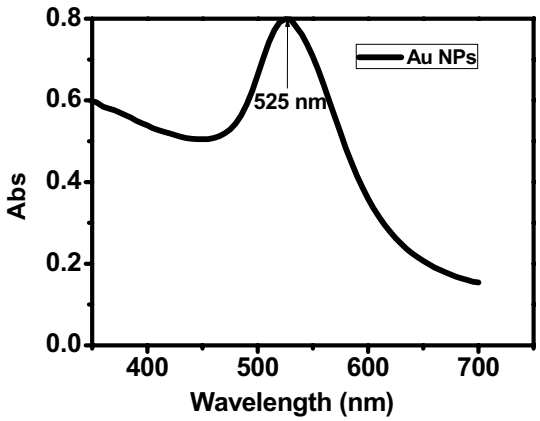

Fig. 3 UV–Vis absorption spectrum of gold nanoparticles (AuNPs) as prepared

surface of sputtered gold shown in Fig. 4b. Probably the dip coating needs rough surface to adhere Gn efficiently on the gold surface.

Rough surface is obtained by dip-coated AuNPs on the surface of bare fiber optic core, as shown in Fig. 4d. The difference of surface roughness is clear between the images in Fig. 4b, d respectively. Gn deposited on the dip-coated AuNPs on the surface of bare fiber optic core is clearly shown in Fig. 4e, and the roughness of Gn surface is shown.

The surface shape in image in Fig. 4d, e has largest surface area in ascending order, respectively, due to the surface roughness which may be increase the sensor sensitivity.

Raman spectroscopy was used to examine the samples of different structures as shown in Fig. 5. Figure 5a–c shows the Raman spectra for core, Au/core, Gn/Au/core and AuNPs/core, Gn/AuNPs/core and comparison between Raman of Gn/Au/core and Gn/AuNPs/core. The bands of Au/core and AuNPs/core are appearance at (2127 cm^{-1}, 3144 cm^{-1}) and (2134 cm^{-1}, 3160 cm^{-1}), respectively. After the dip coating of graphene on Au/core and AuNPs/core surfaces, the appearance of D (1337 cm^{-1}), G (1568 cm^{-1}) and 2D (2693 cm^{-1}) bands for Gn/Au/core and the appearance of D (1347 cm^{-1}), G (1570 cm^{-1}) and 2D (2700 cm^{-1}) bands for Gn/AuNPs/core revealed the deposition of graphene on Au/core and AuNPs/core surfaces. From Fig. 5, the intensities of D, G and 2D peak of graphene are enhanced; this may be caused by electromagnetic enhancement from gold and electron transfer between gold and graphene. The high intensity and shift of the D peak indicate that the process of the gold coating may introduce some defects on the graphene. A slight shift of 2D peak may be related to the electron transfer between graphene and gold. The close contact of gold with graphene makes electromagnetic enhancement more active. We concluded that the defects of graphene introduced in the dip coating method improve the ability to trap lead ions.

3.2 Sensing experimental results

After preparing four different sensing probes (Au film/core, AuNPs/core, Gn/Au/core and Gn/AuNPS/core). The

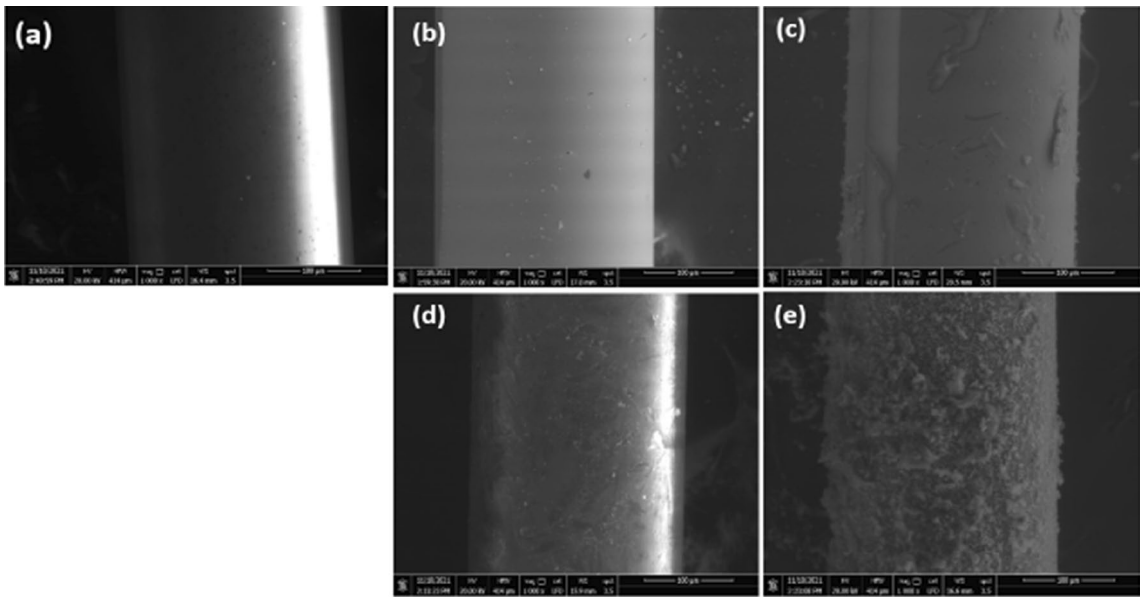

Fig. 4 SEM images for (**a**) unclad core of the optical fiber, (**b**) Au/core, (**c**) Gn/Au/core, (**d**) AuNPs/core and (**e**) Gn/AuNPs/core. The images are at the scale of 100 µm

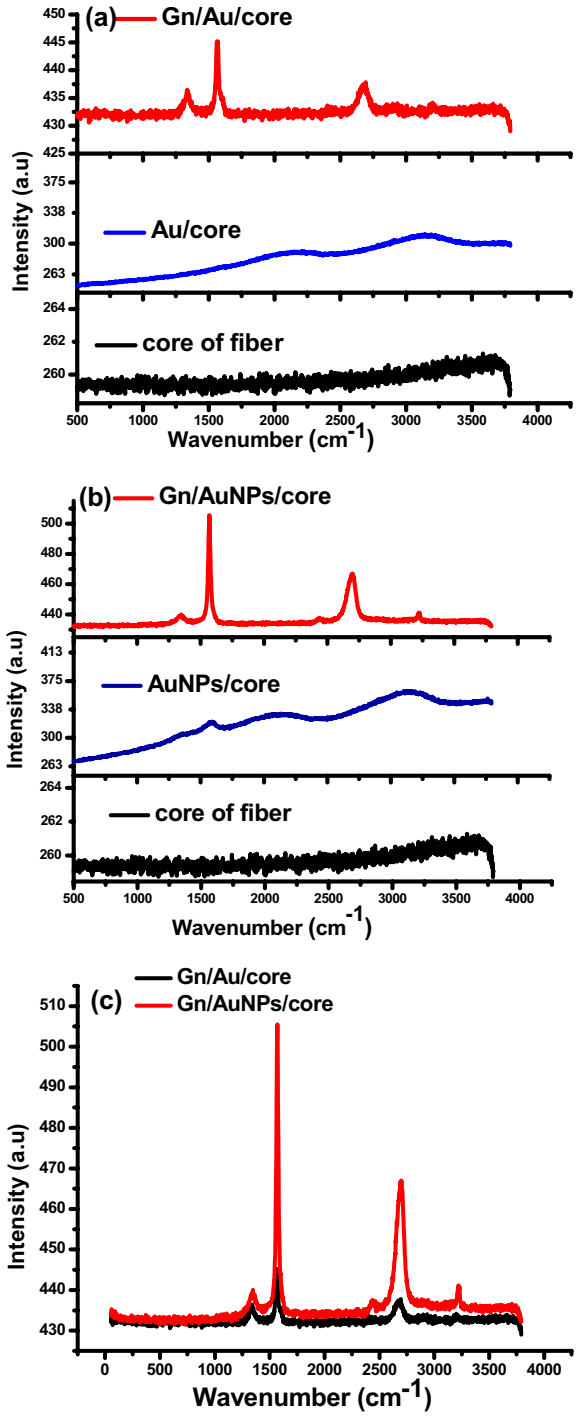

Fig. 5 Raman spectra for (**a**) core of optical fiber, Au/core and Gn/Au/core (**b**) core of optical fiber, AuNPs/core and Gn/AuNPs/core (**c**) comparison between Raman of Gn/Au/core and Gn/AuNPs/core

probes are fixed in axial part of the cell as shown in Fig. 2. SPR curve was measured for different concentrations of lead metal ions. The SPR spectrum is the ratio between the transmission spectrums of the sensed medium and the transmission spectrum in the absence of sensed medium [38]. Water was used as a reference, and the spectrum for different concentrations of lead ions in water were recorded for the four sensing probes used as shown in Fig. 6.

In the SPR curve, a sharp dip occurs in transmission at the specific wavelength called the resonance wavelength. The position of this dip is dependent upon the sensed medium refractive index. With increasing the concentration of lead ions in water, the SPR curves for four sensor probes are redshifted to higher wavelengths. The resonance wavelengths were determined from minimum of SPR curves for all sensor probes for different lead ion concentrations as shown in Fig. 6a–d. To compare the sensing of the prepared four probes, we study the sensing characteristics of Au film and AuNPs without/with graphene. As shown in Fig. 7a, as lead ion concentrations increase, the resonant wavelength is redshifted 13 nm from 641 to 654 nm for the Au/core and 22 nm from 648 to 670 for Gn/Au/core. Also as the lead ion concentrations increase, the resonant wavelength are redshifted 17 nm from 642 to 659 nm for the AuNPs/core probe and 42 nm from 680 to 722 nm for Gn/AuNPs/core probe as shown in Fig. 7b. In Gn/Au/core and Gn/AuNPs/core fiber optic SPR sensors, the position of resonant wavelength is greater than that of the sensor without graphene, which is due to the large real part of the dielectric function of graphene layer [39]. Such results show that the presence of graphene improves SPR fiber optic sensor resolution.

With the presence of graphene as a sensing layer, the bandwidth (FWHM) is widened as shown in Fig. 8a, b. FWHM of the Gn/Au/core and Gn/AuNPs/core of fiber optic SPR sensors is larger than that of the Au/core and AuNPs/core sensors at the same lead ion concentration. Moreover, Fig. 8a, b reveals there has been marked increase in the bandwidth (FWHM) with lead ion concentration increase.

Also, the presence of graphene in sensor structure shows a noticeable increase in transmission intensity of SPR spectra sensors, comparable with the sensors without graphene as shown in Fig. 9a, b. From Fig. 9a, b, the Gn/AuNPs/core sensor shows a higher minimum transmission intensity (at different resonance wavelengths) than the minimum transmission Intensity of other sensors even for Gn/Au/core.

What stands out in Fig. 9a is the dramatic decline in the minimum intensity for both Au/core and Gn/Au/core structures compared to AuNPs/core and Gn/AuNPs/core in range (0–50 ppm).

This is may be due to the smooth surfaces of both Au/core and Gn/Au/core as shown in SEM images (Fig. 4b, c, Sect. 3.1).

In Fig. 9a, the nearly coincide curves for sensor with Au/core and Gn/Au/core, this may be due to the faint layer of graphene, as shown in SEM images (Fig. 4b, c, Sect. 3.1).

In contrast, in Fig. 9b there is a jump growth in intensity for Gn/AuNPs/core relative to the AuNPs/core due to high roughness of the graphene layer surface, which increase the

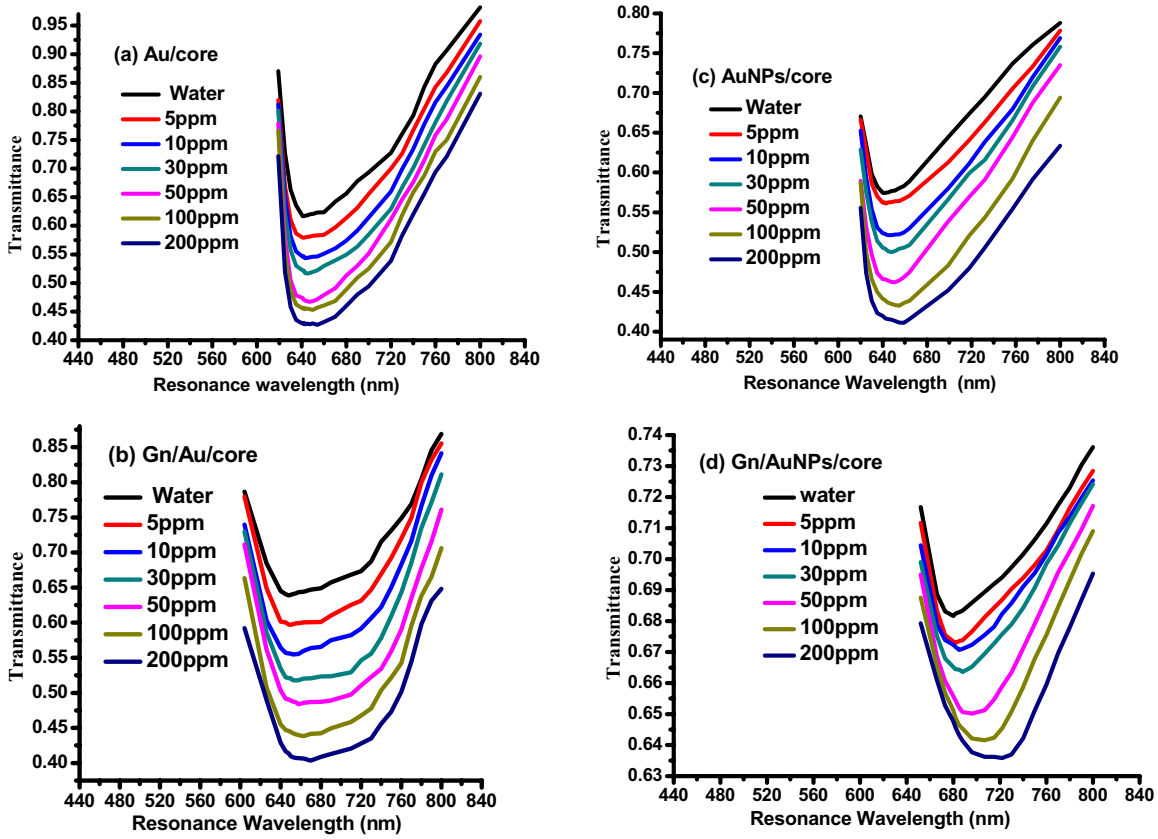

Fig. 6 Transmission spectra of prepared sensing probes for (**a**) Au/core, (**b**) Gn/Au/core, (**c**) AuNPs/core and (**d**) Gn/AuNPs/core

surface area. Also this jump in case of graphene may be due to affinity of Gn surface in this case to lead ions.

3.3 Performance parameters analysis

Usually, the performance of SPR sensors is evaluated using the four key parameters: sensitivity (Sn), figure of merit (FOM) (quality factor), signal-to-noise ratio (SNR) and limit of detection (LOD), all of which should be held as high as possible to achieve greater efficiency.

Sensitivity (Sn) measures the ability of sensing the change in refractive index of sensing medium due to the molecule absorption.

Sensitivity (Sn) and figure of merit (FOM) are calculated using Eqs. (2) and (3), respectively [40].

$$\mathrm{Sn} = \Delta\lambda_{\mathrm{res}}/\Delta c \tag{2}$$

where Δc is the change in the concentration of the solution and $\Delta\lambda_{\mathrm{res}}$ is the shift in the corresponding resonant wavelength.

$$\mathrm{FOM} = \mathrm{Sn}/\mathrm{FWHM} \tag{3}$$

where Sn is the sensitivity and FWHM is the width of the spectral curve.

To evaluate the sensitivity of the fiber optic SPR sensor, the resonant wavelengths of the fiber optic SPR sensors with and without graphene as a function of concentrations are plotted in Fig. 8a, b and fitted linearly as shown in Fig. 10a, b and the slope is the sensitivity of the sensing probe. From Fig. 10a, b, the calculated sensitivity was 0.06307, 0.08324 and 0.10483, 0.21 nm/ppm for Au/core, AuNPs/core, Gn/Au/core and Gn/AuNPs/core, respectively. It is clear that graphene improves the sensitivity efficiently, and Gn/AuNPs/core and Gn/Au/core have enhanced sensitivity 252% and 166% with respect to that of AuNPs/core and Au/core probes. This enhancement is better than the probes coated by transferring CVD graphene as reported [32, 41].

Depending on the sensitivity of the sensor and the full width at half maximum (FWHM) of the SPR transmission spectrum, the figure of merit can be calculated as FOM = S/FWHM. The FWHM of four fiber optic SPR sensors is shown in Fig. 6a–d respectively. All the values of figure of merit for the four sensors are labeled in Table 1, which shows the increase in figure of merit with the existence of graphene despite the broadening of FWHM due to graphene; this means that the increase in the sensitivity weakens the role

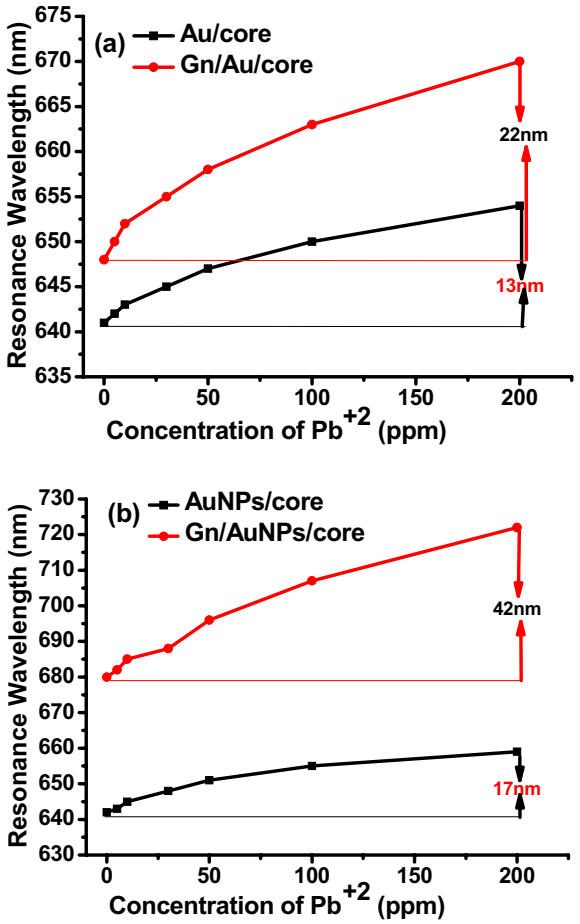

Fig. 7 **a**, **b** Variation of resonance wavelength with the concentrations of lead ions for sensing probes: (**a**) Au/core and Gn/Au/core, and (**b**) AuNPs/core and Gn/AuNPs/core

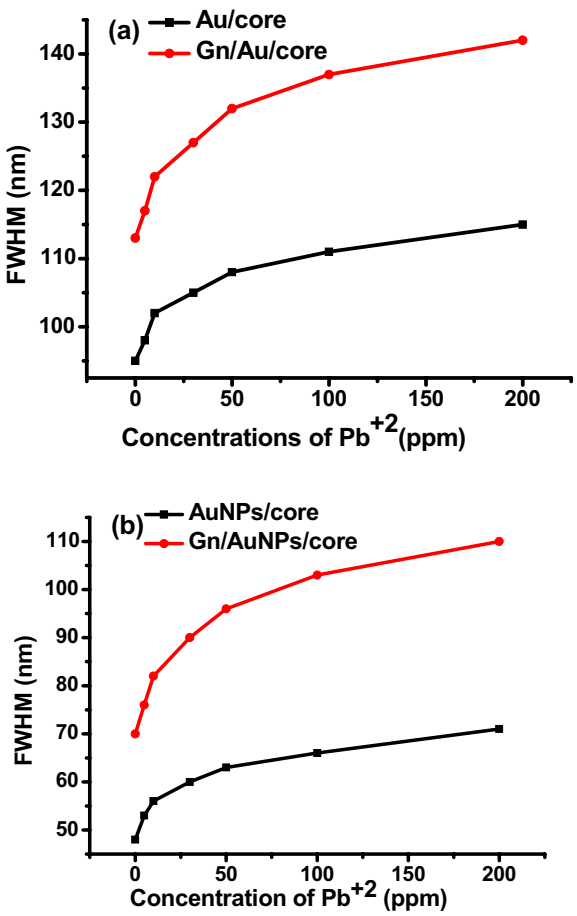

Fig. 8 **a**, **b** Variation of band width (FWHM) with the concentrations of lead ions for sensing probes: (**a**) Au film and Gn/Au/core, and (**b**) AuNPs/core and Gn/AuNPs/core

of broadening of FWHM in Eq. (3). The calculated FOM values of the Gn/Au/core and Gn/AuNPs/core fiber optic SPR sensors are 36.3×10^{-4} ppm^{-1} and 52.5×10^{-4} ppm^{-1}, respectively, which are larger than 31.5×10^{-4} ppm^{-1} and 36×10^{-4} ppm^{-1} of the Au/core and AuNPs/core fiber optic SPR sensors, respectively. It is clear that graphene improves the figure of merit efficiently; Gn/AuNPs/core and Gn/Au/core have enhanced figure of merit 146% and 115% with respect to that of AuNPs/core and Au/core probes.

The signal-to-noise ratio (SNR) is another performance parameter that combines the effect of SPR resonance wavelength shift ($\Delta\lambda_{res}$) and detection accuracy (DA) and is determined by multiplying ($\Delta\lambda_{res}$) of SPR by DA, where detection accuracy is the ability of monitor the minimum change in the refractive index of the sensing medium. It is measured as the change in the resonance wavelength to FWHM. The SNR of the Au/core, Gn/Au/core, AuNPs/core and Gn/AuNPs/core sensors for Pb^{+2} metal ions is depicted in Fig. 11a, b. The SNR for all four SPR sensors clearly increases as the Pb^{+2} concentration increases. For each concentration of lead ions, the SNR of the Gn/Au/core and Gn/AuNPs/core sensors is higher than that of the Au/core and AuNPs/core sensors. Table 1 demonstrates the increase in signal-to-noise ratio (SNR) with the presence of graphene by labeling the high SNR values for four sensors. It is clear that the SNR of Gn/AuNPs/core and Gn/Au/core have enhanced signal-to-noise ratio 266% and 167% with respect to that of AuNPs/core and Au/core probes. The Gn/AuNPs/core fiber optic SPR sensor has the best SNR for each concentration, which is due to the higher affinity of Gn/AuNPs/core than the other sensors. As a result of this finding, SNR is another indicator of binding affinity because the quantity is highly dependent on the $\Delta\lambda_{res}$ of SPR [47]. This also indicates that the shape of SNR curve is affected by the shift in the SPR wavelength, indicating that $\Delta\lambda_{res}$ of SPR has a greater influence on SNR value than DA.

Limit of detection (LOD) of a sensor is defined as the lowest concentration of analyte, which can be detected by the sensor with good accuracy. It can be calculated by using Eq. (5) [40].

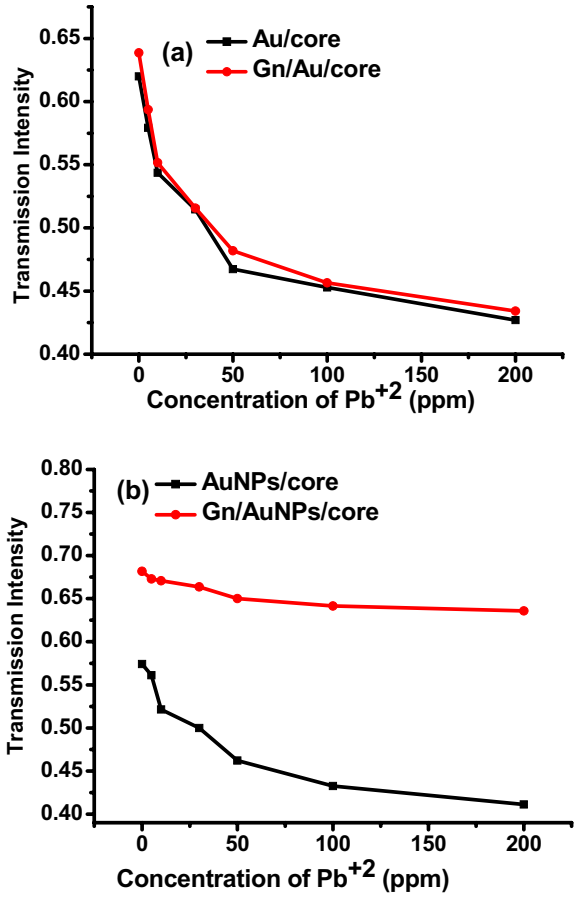

Fig. 9 **a**, **b** Variation of transmission dip (I_{min}) with the concentrations of lead ions for sensing probes: (**a**) Au/core and Gn/Au/core, and (**b**) AuNPs/core and Gn/AuNPs/core

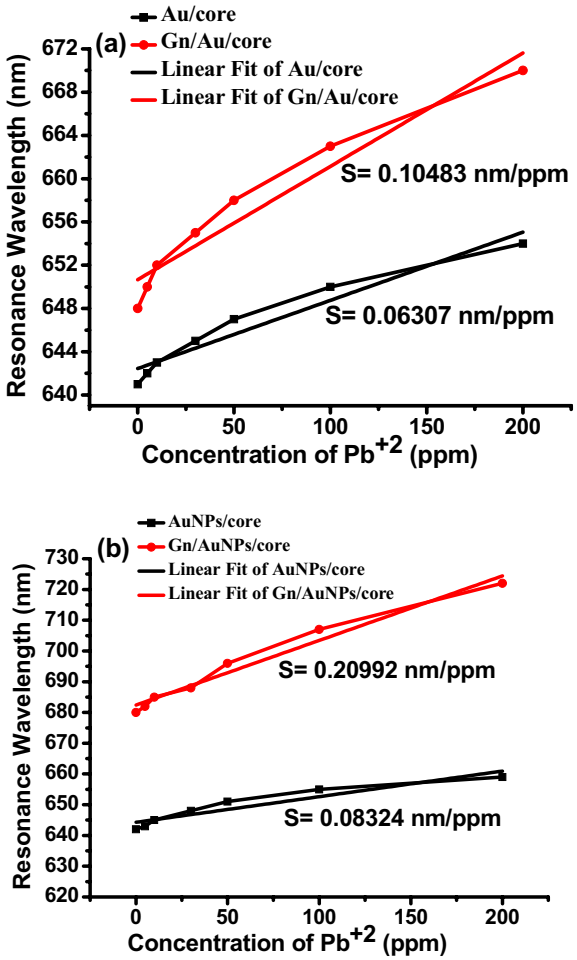

Fig. 10 **a, b** Liner fitting of wavelength resonance as a function of concentrations for four sensors: (**a**) Au/core, Gn/Au/core, (**b**) AuNPs/core and Gn/AuNPs/core

$$\mathrm{LOD} = \Delta\lambda s/\mathrm{Sn} \tag{5}$$

where $\Delta\lambda s$ is the resolution of spectrometer which equal to 0.1 nm in our experiment and Sn is the sensitivity of the sensor near zero concentration.

LODs of the Au/core and AuNPs/core fiber optic SPR sensors are 1.6 ppm and 1.2 ppm, respectively, which are larger than that 0.95 ppm and 0.48 ppm of the Gn/Au/core and Gn/AuNPs/core fiber optic SPR sensors, respectively, as labeled in Table 1. As shown in Table 1, graphene enhances the limit of detection of fiber optic sensors, and the Gn/AuNPs/core fiber optic SPR sensor has the best limit of detection.

The sensor should be high selective toward the aimed analyte. Selectivity is confirmed through the difference of the resonance wavelength equivalent maximum and zero concentration of the target analyte. Here, a selective sensor shows a maximum shift in resonance wavelength for the analyte [48].

For our case, the maximum shift in resonance wavelengths for lead ion concentrations (0–200 ppm) was 42, 22, 17 and 13 nm for Gn/AuNPs/core, Gn/Au/core, AuNps/core and Au/core probes, respectively. This indicates that Gn/AuNPs/core sensor is highly selective for lead ions. Semwal et al. [49] show a maximum shift in the resonance wavelengths of 32, 1, 2 and 3 nm for H_2O_2, sucrose, urea and ascorbic acid, respectively. Their senor was gold–graphene oxide (GO) layers followed by the immobilization of catalase enzyme. This proves their sensor is selective for H_2O_2. On the other hand, SPR fiber optic sensor is designed to measure one element such as lead ions and glucose, while the measurements of different elements at the same time are difficult with these SPR sensors.

Figure 12 includes in brief that the dip-coated graphene enhances the all parameters of fiber optic sensors (FOS). The Gn/AuNPs/core sensor has the best performance parameters than other sensors. In comparison with earlier sensors, our Gn/AuNPs/core sensor has a sensitivity of 0.21 nm/ppm, which is greater than the sensitivity values of other works

Table 1 Comparison of the fabricated sensing sensors in this work with other works for lead ion detections

Sensing materials for optical fiber sensor	Operating range	Sensitivity	SNR	LOD	FOM (ppm^{-1})	References
Chitosan-coated sensor	0–70 ppm	0.044 dBm/ppm	–	–	–	[42]
chitosan and glutathione	1–7 ppb	0.28 mV/ppb	–	1.3 ppb	–	[43]
Au/γ – Fe2O3/rGO	0–15 ppm	0.0012 nm/ppm	–	–	–	[44]
AuNP-coated fiber	0–100 mM	0.28 nm/mM	–	65 ppm	–	[45]
pyrrole/chitosan/ITO/Ag	0–200 µg/L	0.00075 nm/ppm	–	0.44 ppb	–	[46]
Au/core	0–200 ppm	0.063 nm/ppm	0.12	1.58 ppm	0.0031	This work
Gn/Au/core	0–200 ppm	0.11 nm/ppm	0.2	0.95 ppm	0.0037	This work
AuNPs/core	0–200 ppm	0.083 nm/ppm	0.14	1.2 ppm	0.0036	This work
Gn/AuNPs/core	0–200 ppm	0.21 nm/ppm	0.4	0.48 ppm	0.0053	This work

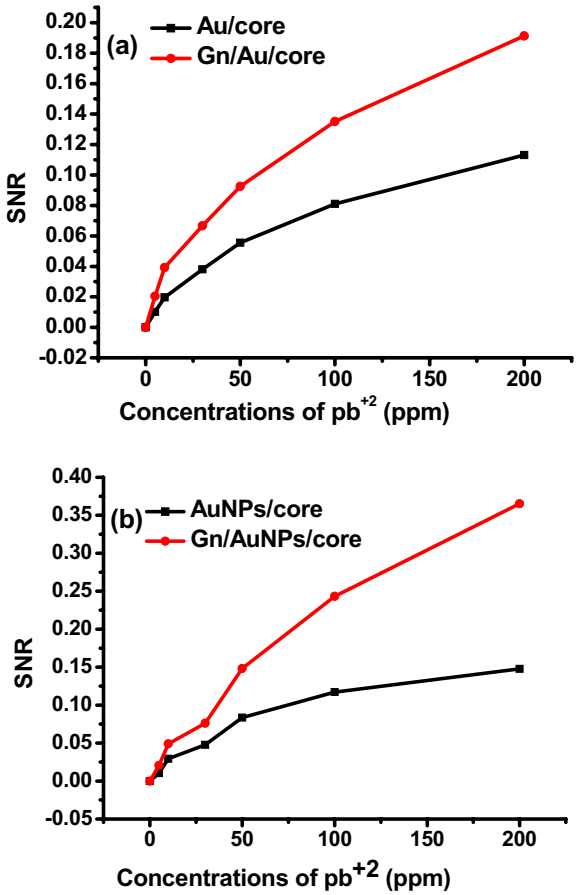

Fig. 11 **a, b** Signal-to-noise ratio for four sensors in Pb^{+2} ion sensing (**a**) Au/core, Gn/Au/core (–) AuNPs/core, Gn/AuNPs/core

as indicated in Table 1. Aside from being less costly, the dip-coated sensor is also easy to handle and environmentally friendly. In Table 1, the sensing parameters of all proposed sensors are compared to those found in the literature.

In future work, we have interest to fabricate SPR fiber optic sensing probes using two-dimensional (2D) transition–metal dichalcogenide (TMDC) materials such as tungsten disulfide (WS_2), tungsten selenide WSe_2, molybdenum selenide $MoSe_2$ and molybdenum disulfide MoS_2. Recent studies have been modeled and fabricated fiber optic SPR sensors using 2D TMDC materials [50–55]. They found using 2D TMDC enhances SPR fiber optic sensor performance due to their remarkable electrical and optical properties. These studies provide us support for fabricating new sensing probes using 2D TMDC materials by dip coating technique.

4 Conclusions

This study is set out to enhance performance of fiber optic SPR probes. Different sensing probes of Au/core, Gn/Au/core, AuNPs/core and Gn/AuNPs/core were prepared and were investigated via SEM and Raman spectroscopy. Detection of lead ions with different concentrations was examined with the prepared probes. Redshifted SPR spectra of all the probes are observed with Pb^{+2} ion increase. The contribution of this study has been to confirm the role of dip-coated graphene for enhancing the performance of probes. The performance of the probes, in terms of Sn, FOM, SNR and LOD, were discussed, and significance performances are recorded for Gn/Au/core and Gn/AuNPs/core probes than Au/core and AuNPs/core probes, respectively. We concluded that the superior sensing parameters of Gn/AuNPs/core probe were a sensitivity of 0.21 nm/ppm, FOM (52.5×10^{-4} ppm^{-1}), SNR (0.366) and LOD 0.48 ppm. The key strengths of this study are low-cost dip coating method and remarkable enhancement of sensing due to graphene. A natural progression of this work is preparing other sensing probes using graphene probe with different structures.

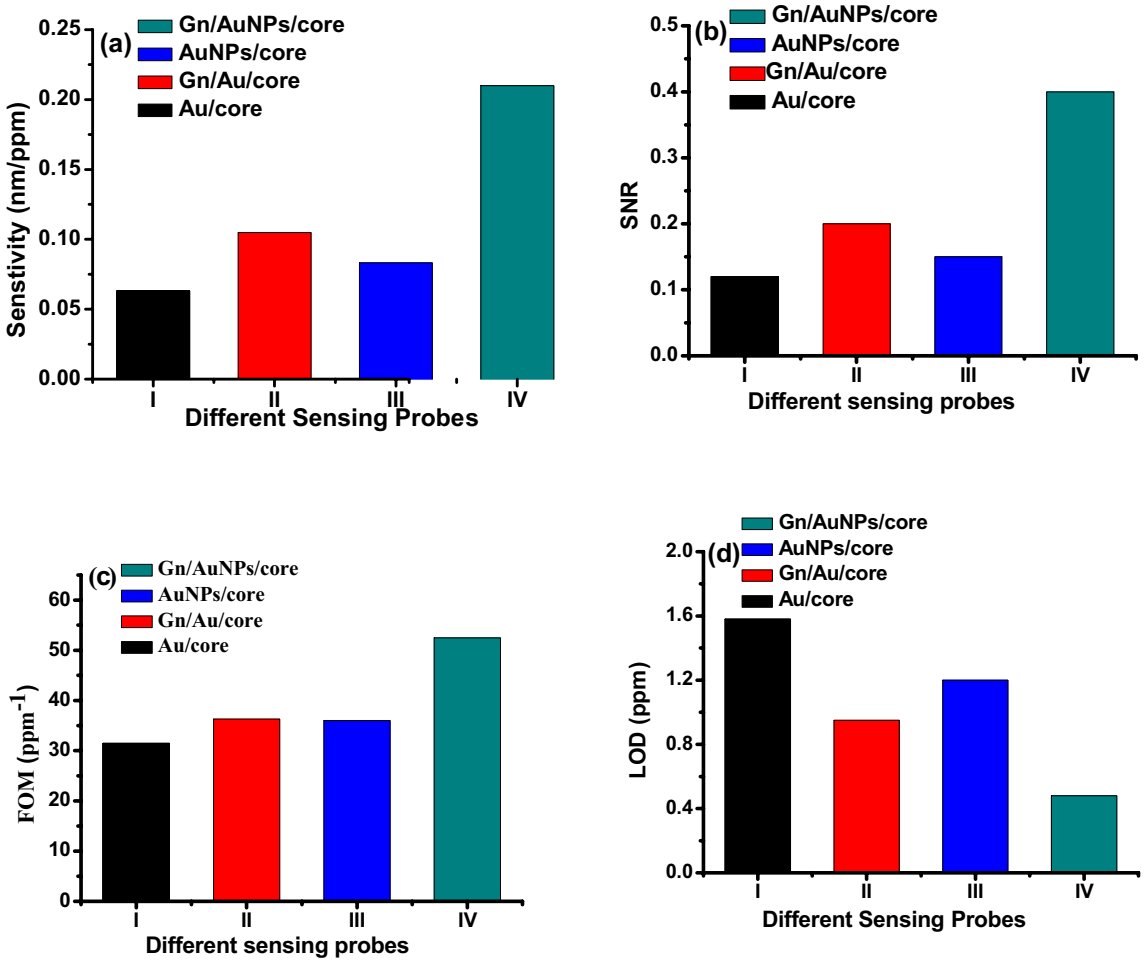

Fig. 12 Performance parameters for the prepared four sensors

References

1. P. Lecaruyer, M. Canva, J. Rolland, Metallic film optimization in a surface plasmon resonance biosensor by the extended Rouard method. Appl. Opt. **46**, 2361–2369 (2007)
2. C. Perrotton, N. Javahiraly, M. Slaman, B. Dam, P. Meyrueis, Fiber optic surface plasmon resonance sensor based on wavelength modulation for hydrogen sensing. Opt. Express. **19**, A1175–A1183 (2011)
3. S. Deng, P. Wang, X. Yu, Phase-sensitive surface plasmon resonance sensors: recent progress and future prospects. Sensors **17**, 2819 (2017)
4. M.H.H. Hasib, J.N. Nur, C. Rizal, K.N. Shushama, Improved transition metal dichalcogenides-based surface plasmon resonance biosensors. Condensed Matter. **4**(2), 49 (2019)
5. Y.H. Huang, H.P. Ho, S.K. Kong, A.V. Kabashin, Phase-sensitive surface plasmon resonance biosensors: methodology, instrumentation and applications. Ann. Phys. **524**(11), 637–662 (2012)
6. J. Homola, On the sensitivity of surface plasmon resonance sensors with spectral interrogation. Sens. Actuators Chem. **41**(1–3), 207–211 (1997)
7. H. Vahed, C. Nadri, Ultra-sensitive surface plasmon resonance biosensor based on MoS2 graphene hybrid nanostructure with silver metal layer. Opt. Quant. Electron. **51**(1), 1–13 (2019)
8. Z. Salamon, H. Angus-Macleod, G. Tollin, Surface plasmon resonance spectroscopy as a tool for investigating the biochemical and biophysical properties of membrane protein systems. Biochimica ET Biophysica Acta Reviews on Biomembranes. **1331**(2), 131–152 (1997)
9. A.K. Sharma, B.D. Gupta, On the performance of different bimetallic combinations in surface plasmon resonance based fiber optic sensors. J. Appl. Phys. **101**, 093111 (2007)
10. S.K. Srivastava, B.D. Gupta, Influence of ions on the surface plasmon resonance spectrum of a fiber optic refractive index sensor. Sensors Actuators B Chem. **156**(2), 559–562 (2011)
11. J.C. Hsu, S.W. Jeng, Y.S. Sun, Simulation and experiments for optimizing the sensitivity of curved D-type optical fiber sensor with a wide dynamic range. Opt Commun. **341**, 210–217 (2015)
12. E. Wijaya, C. Lenaerts, S. Maricot, J. Hastanin, S. Habraken, J.-P. Vilcot, R. Boukherroub, S. Szunerits, Surface plasmon resonance-based biosensors: From the development of different SPR structures to novel surface functionalization strategies. Curr. Opin. Solid State Mater. Sci. **15**, 208–224 (2011)
13. A. Nisha, P. Maheswari, P.M. Anbarasan, K.B. Rajesh, Z. Jaroszewicz, Sensitivity enhancement of surface plasmon resonance sensor with 2D material covered noble and magnetic material (Ni). Opt. Quant. Electron. **51**, 1 (2019)

14. M.S. Rahman, M.R. Hasan, K.A. Rikta, M.S. Anower, A novel graphene coated surface plasmon resonance biosensor with tungsten disulfide (WS_2) for sensing DNA hybridization. Opt. Mater. **75**, 567–573 (2018)
15. E. Kretschsmann, H. Reather, Radiative decay of non-radiative surface plasmons exited by light. Zeitschrift fur nature forschung **23**, 2135–2136 (1968)
16. Q. Wang, J.Y. Jing, X.Z. Wang, L.Y. Niu, W.M. Zhao, A D-shaped fiber long-range surface plasmon resonance sensor with high Q-factor and temperature self-compensation. IEEE Trans. Instrum. Meas. **69**, 2218–2224 (2020)
17. F. Xia, H. Song, Y. Zhao, W.M. Zhao, Q. Wang, X.Z. Wang, B.T. Wang, Z.X. Dai, Ultra-high sensitivity SPR fiber sensor based on multilayer nanoparticle and Au film coupling enhancement. Measurement **164**, 108083 (2020)
18. C. Nylander, B. Liendberg, T. Lind, Gas detection by means of surface plasmons resonance. Sens. Actuators **3**, 79–88 (1982)
19. R.C. Jorgenson, S.S. Yee, A fiber-optic chemical sensor based on surface plasmon resonance. Sens. Actuators, B. **12**, 213–220 (1993)
20. R. Slavík, J. Homola, J. Ctyroky, E. Brynda, Novel spectral fiber optic sensor based on surface plasmon resonance. Sens. Actuators B. **74**, 106–111 (2001)
21. S. Rajan, B. Chand, D. Gupta, Surface plasmon resonance based fiber-optic sensor for the detection of pesticide. Sens. Actuators B. **123**, 661–666 (2007)
22. Q. Wang, J.-Y. Jing, W.-M. Zhao, X.-C. Fan, X.-Z. Wang, A novel fiber-based symmetrical long-range surface plasmon resonance biosensor with high quality factor and temperature self-reference. IEEE Trans. Nanotechnol. **18**, 1137–1143 (2019)
23. J. Yao, M.J. StewartME, T.W. Lee, S.K. Gray, J.A. Rogers, R.G. Nuzzo, Seeing molecules by eye: surface plasmon resonance imaging at visible wavelengths with high spatial resolution and submonolayer sensitivity. Angew. Chem. Int. Ed. **47**(27), 5013–5017 (2008)
24. P. Bhatia, B.D. Gupta, Fabrication and characterization of a surface plasmon resonance based fiber optic urea sensor for biomedical applications. Sensors Actuators B Chem. **161**(1), 434–438 (2012)
25. A. Hanning, J. Roeraade, J.J. Delrow, R.C. Jorgenson, Enhanced sensitivity of wavelength modulated surface plasmon resonance devices using dispersion from a dye solution. Sens. Actuators B. **158**, 372–376 (2011)
26. N. Reckinger, A. Vlad, S. Melinte, J.-F. Colomer, M.L. Sarrazin, Graphene-coated holey metal films: tunable molecular sensing by surface plasmon resonance. Appl. Phys. Lett. **102**, 211108 (2013)
27. X.F. Wang, Plasmon spectrum of two-dimensional electron systems with Rashba spin-orbit interaction. Phys. Rev. B **72**(8), 085317 (2005)
28. Y. Liu, X. Dong, P. Chen, Biological and chemical sensors based on graphene materials. Chem Soc Rev. **41**(6), 2283–2307 (2012)
29. M. Kim, C.Y. Jeong, H. Heo, S. Kim, Optical reflection modulation using surface plasmon resonance in a graphene-embedded hybrid plasmonic waveguide at an optical communication wavelength. Opt Lett. **40**(6), 871–874 (2015)
30. Z.H. Ni, H.M. Wang, J. Kasim, H.M. Fan, T. Yu, Y.H. Yu, Y.P. Feng, Z.X. Shen, Graphene thickness determination using reflection and contrast spectroscopy. Nano Lett. **7**, 2758–2763 (2007)
31. D.W. Horsell, P.J. Hale, A.K. Savchenko, Mechanical manipulation and measurement of graphene by atomic force microscopy. Microscopy Anal. **25**, 9–11 (2011)
32. W. Wei, J. Nong, Y. Zhu, G. Zhang, N. Wang, S. Luo, N. Chen, G. Lan, C.J. Chuang, Y. Huang, Graphene/Au-enhanced plastic clad silica fiber optic surface plasmon resonance sensor. Plasmonics. **13**, 483–491 (2018)
33. O. Salihoglu, S. Balci, C. Kocabas, Plasmon-polaritons on graphene-metal surface and their use in biosensors. Appl. Phys. Lett. **100**(21), 213110 (2012)
34. M. Gomaa, G.A. Fattah, Synthesis of graphene and graphene oxide by microwave plasma chemical vapor deposition. J Am Sci. **12**(3), 72–80 (2016)
35. G. Frens, Controlled nucleation for the regulation of the particle size in monodiperse gold suspensions. Nat. Phys. Sci. **241**(105), 20–22 (1973)
36. M. Gomaa, G.A. Fattah, Optical properties of graphene oxide thin film reduced by low cost diode laser. Appl. Phys. A **126**(7), 519 (2020)
37. J.P. Anhalt, J.A. Washington II., Preparation and storage of antimicrobials, in *Manual of clinical microbiology*, 5th edn., ed. by W.J. Hausler, K.L. Herrmann, H.D. Isenberg, H. Shadomy (American Society for Microbiology, Washington, DC, 1991), pp. 1199–1200
38. M.F. Sultan, A.A. Al-Zuky, S.A. Kadhim, Surface plasmon resonance based fiber optic sensor: theoretical simulation and experimental realization. J. Al-Nahrain Univ. **21**(1), 65–70 (2018)
39. P.K. Maharana, T. Srivastava, R. Jha, On the performance of highly sensitive and accurate graphene-on-aluminum and silicon based SPR biosensor for visible and near infrared. Plasmonics **9**(5), 1113–1120 (2014)
40. N. Cennamo et al., Low cost sensors based on SPR in a plastic optical fiber for biosensor implementation. Sensors **11**(12), 11752–11760 (2011)
41. Y. Zhao, S.-Y. Zhang, G.-F. Wen, Z.-X. Han, Graphene-based optical fiber ammonia gas sensor. Instrum Sci. Technol. **46**(1), 12–27 (2017)
42. N.M. Razali, N.F. Zaidi, P.N. Jaafar, A. Hamzah, F. Ahmad, S. Ambran, Optical fiber tip sensor coated with chitosan for lead ion detection. AIP Publish. **2203**, 020035 (2020)
43. B.S. Boruah, R. Biswas, An optical fiber based surface plasmon resonance technique for sensing of lead ions: a toxic water pollutant. Opt. Fiber Technol. **46**, 152–156 (2018)
44. F.H. Suhailin, A.A. Alwahib, Y. Mustapha-Kamil, M.H. Abu-Bakar, N.M. Huang, M.A. Mahdi, Fiber-based surface plasmon resonance sensor for lead ion detection in aqueous solution. Plasmonics **15**, 1369–1376 (2020)
45. P. Dhara, R. Kumar, L. Binetti, H.T. Nguyen, L.S. Alwis, T. Sun, K.T.V. Grattan, Optical fiber-based heavy metal detection using the localized surface plasmon resonance technique. IEEE Sensors (2019). https://doi.org/10.1109/JSEN.2019.2921701
46. R. Verma, B.D. Gupta, Detection of heavy metal ions in contaminated water by surface plasmon resonance based optical fibre sensor using conducting polymer and chitosan. Food Chem. **166**, 568–575 (2015)
47. N. Cennamo, D. Massarotti, R. Galatus, L. Conte, L. Zeni, Performance comparison of two sensors based on surface plasmon resonance in a plastic optical fiber. Sensors **13**, 721–735 (2013)
48. R. Tabassum, R. Kant, Recent trends in surface plasmon resonance based fiber–optic gas sensors utilizing metal oxides and carbon nanomaterials as functional entities. Sensors Actuators B Chem. **310**, 127813 (2020)
49. V. Semwal, B.D. Gupta, Highly selective SPR based fiber optic sensor for the detection of hydrogen peroxide, sensors Actuators. B Chem. **329**, 129062 (2021)
50. W. Wei, J. Nong, L. Tang, N. Wang, C.J. Chuang, Y. Huang, Graphene-MoS_2 hybrid structure enhanced fiber optic surface plasmon resonance sensor. Plasmonics **12**, 1205–1212 (2017)
51. Y. Cai, W. Li, Y. Feng, J.S. Zhao, G. Bai, J. Xu, J.Z. Li, Sensitivity enhancement of WS2-coated SPR-based optical fiber biosensor for detecting glucose concentration. Chin. Phys. B. **29**, 110701 (2020)
52. C. Odacı, U. Aydemir, The surface plasmon resonance-based fiber optic sensors: a theoretical comparative study with 2D TMDC materials. Results Opt. **3**, 100063 (2021)

53. J.K. Nayak, P.K. Maharana, R. Jha, Dielectric over-layer assisted graphene, its oxide and MoS2-based fibre optic sensor with high field enhancement. J. Phys. D. Appl. Phys. **50**, 405112 (2017)
54. S. Kaushik, U.K. Tiwari, S.S. Pal, R.K. Sinha, Rapid detection of Escherichia coli using fiber optic surface plasmon resonance immunosensor based on biofunctionalized Molybdenum disulfide (MoS_2) nanosheets. Biosens. Bioelectron. **126**, 501–509 (2019)
55. S. Kumar, Z. Guo, R. Singh, Q. Wang, B. Zhang, S. Cheng, F.Z. Liu, C. Marques, B.K. Kaushik, R. Jha, MoS_2 Functionalized multicore fiber probes for selective detection of shigella bacteria based on localized plasmon. J. Light. Technol. **39**, 4069–4081 (2021)